LA-UR-01-3737
Approved for public release;
distribution is unlimited.

Title: **ADTF SUPERCONDUCTING LINAC DESIGN**

Author(s): Robert Garnett

Submitted to:

http://lib-www.lanl.gov/la-pubs/00796672.pdf

Los Alamos
NATIONAL LABORATORY
memorandum

Los Alamos Neutron Science Center, LANSCE-1
Accelerator Physics and Engineering Group

To/MS: Distribution
From/MS: Robert Garnett, H817
Phone/Fax: 5-2835/5-2904
Symbol: LANSCE-1:01-047
Date: May 1, 2001
Email: rgarnett@lanl.gov

SUBJECT: ADTF SUPERCONDUCTING LINAC DESIGN

The ADTF superconducting linac design discussed here is the one presented recently at the AAA/ADTF Linac Design Review on April 10-12, 2001. Many of the details of the design have already been documented in a previous memorandum [1] containing the viewgraphs presented at the review. For completeness, I have included some of the same information along with a discussion of the design parameters and simulation results. The superconducting design presented here to accelerate a beam from 6.7-600 MeV can meet the requirements for a 13.3-mA ADTF facility. Additional design work will be required to reduce beam losses observed in the simulations if 100-mA operation is required for tritium production. At 13.3 mA, this design was shown to have an inherent tolerance for RF system component failures and magnet failures.

Accelerator Layout and Design Details

Table 1 shows the accelerator layout. We have assumed that the input beam for this linac is the output beam from the existing LEDA RFQ. The cryomodule and cryoperiod dimensions were determined through an iterative process involving Phillip Roybal (LANSCE-1 Mechanical Designer) and Patrick Kelley (LANSCE-1 Cryogenics Engineer). In order to minimize the cryomodule length, a relatively detailed engineering layout of the cryomodule was required and is documented in a memorandum [2]. The dimensions resulting from this layout are also given in Table 1. Transverse focusing is achieved in the first 4 sections through the use of superconducting solenoids inside the cryostat. The last section uses room-temperature quadrupole doublets between the cryomodules for beam focusing. Figure 1 shows the schematic cryomodule layout for each section of the linac.

After the cryomodule layout had been established as discussed above, the design parameters were chosen so as to capture the RFQ beam and to efficiently accelerate the beam to 600 MeV. This was done while trying also to avoid beam envelope instabilities and to provide a current-independent focusing lattice. Our studies showed that at low beam velocities we could not readily take full advantage of the high accelerating gradients available with superconducting cavities. We found it necessary to adiabatically ramp the accelerating gradients to avoid excessively high longitudinal phase advances and resulting beam losses. It should be noted that our choice of parameters is probably not yet optimized.

A scheme for beam matching from the RFQ to the SC linac will be required. There are several possible ways to do this. This work is presently in progress, however, a method to do the matching using 2 cavities and a single solenoid is discussed in a recent memorandum by George Neuschaefer [3]. This method would require re-machining the RFQ vanes so that the exiting beam is round. We will discuss in another section below how the beam matching was done in the simulations.

Appendix A contains the design code output file, SCLINAC.DAT. Detailed beam dynamics design information for the first four sections of the linac is shown including the solenoid values required, the synchronous phase ramping, and design E0 for each cavity. Section 5 of the linac is identical to the baseline APT design except that the operating synchronous phase has been chosen to be -25°. Design parameters for Section 5 are not given here. Appendix B gives the LINAC code input files and Appendix C gives the matched beam parameters for each beam current as determined by TRACE 3-D.

The design E0 value is obviously dependent upon the transit-time factors used for this design having fixed energy-gain per cavity. The maximum transverse phase advance per period is chosen to be 82° and is allowed to vary to maintain a nearly constant transverse phase-advance per unit length in each section. The cryomodules are long. Therefore, a relatively large zero-current transverse phase-advance per period was chosen to provide the strongest possible transverse beam focusing. Figure 2 shows the transverse and longitudinal phase advances per unit length for Sec. 1-4 of our design. Figure 3 shows the range of required superconducting solenoid magnetic fields. The synchronous phase ramping in Sections 1-2 has been chosen to reduce the effects of RF defocusing and to more adiabatically capture the beam longitudinally assuming the input beam is from the LEDA RFQ. In Section 1, the phase is ramped from -45° to -32°. Additionally, to reduce the RF defocusing, the energy-gain per cavity (and hence the peak field per cavity) has been ramped from 0.08 MeV to 0.353 MeV. In Section 2, the synchronous phase is held at a constant value of -32°. In Section 3 it is ramped from -32° to -28°. In Section 4, the synchronous phase is ramped from -28° to -25°. Note that there is a frequency transition from Section 3 to Section 4 from 350 MHz to 700 MHz. Section 4 is the first 700-MHz section. In Section 5, the synchronous phase is held at a constant value of -25°. In Sections 2-5, the accelerating gradient has been chosen to longitudinally match between sections while not exceeding approximately 5 MV/m in Sections 2-3, 6 MV/m in Section 4, and 7 MV/m in Section 5. Figure 4 shows the phase and amplitude ramps.

Simulation Results

Beam dynamics simulations for the superconducting linac were carried out for 0 mA, 13.3 mA, and 100 mA. PARMTEQM simulations were run to generate a 10,000 macroparticle LEDA RFQ output distribution for each beam current. A modified version of the LINAC code that was provided to us by Ken Crandall was used for the superconducting linac simulations. Appendix B contains the LINAC code input files, LINAC.INP and LINAC.DAT. The file, SCLINAC.DAT, contained in Appendix A, is also used as input to the LINAC code. No operational or alignment errors were included in the simulations.

Table 1 – SC Linac Design Parameters, Strawman S2 Design 3

	Section 1	Section 2	Section 3	Section 4	Section 5	Total
Structure Type	2-gap spoke	3-gap spoke	3-gap spoke	5-cell elliptical	5-cell elliptical	
Frequency (MHz)	350	350	350	700	700	
Cavity Geometric Beta	0.175	0.2	0.34	0.48	0.64	
Cavity Bore Radius (cm)	2.0	3.5	4.0	5.0	6.5	
L-cavity (active) (m)	0.100	0.196	0.333	0.514	0.685	
L-cavity (physical) (m)	0.200	0.296	0.433	0.900	1.200	
L-magnet-to-cavity (m)	0.300	0.300	0.300	0.300	0.000	
L-drift1 (m)	0.300	0.300	0.300	0.100	0.616	
L-drift2 (m)	1.113	1.113	1.113	1.088	0.616	
L-magnet (m)	0.150	0.150	0.150	0.250	0.350	
L-warm-to-cold-1 (m)	0.394	0.394	0.394	0.394	0.642	
L-warm-to-cold-2 (m)	0.419	0.419	0.419	0.394	0.642	
L-warm-space (m)	0.300	0.300	0.300	0.300	1.610	
L-cryomodule (m)	4.226	5.802	6.624	6.183	4.571	
L-cryoperiod (m)	4.526	6.102	6.924	6.483	6.181	
L-focusing period (m)	2.263	3.051	3.462	3.338	6.181	
Cav/cryomodule	4	6	6	4	3	
Cav/section	32	48	48	40	93	261
No. of cryomodules	8	8	8	10	31	65
DW/cav (MeV)	0.08 - 0.353	0.335 - 0.778	0.863 - 1.398	0.950 - 2.727	4.219	
Synchronous Phase (deg)	-45 to –32	-32	-32 to -28	-28 to -25	-25	
EoT (MV/m)	1.131 - 4.162	2.015 - 4.681	3.056 - 4.755	2.093 - 5.854	6.796	
Win,section (MeV)	6.7	14.174	43.544	109.043	211.015	
Wout,section (MeV)	14.174	43.544	109.043	211	600	
DW/section (MeV)	7.474	29.37	65.499	101.957	388.985	
Section Length (m)	36.208	48.816	55.392	64.83	191.596	396.842
Coupler Power @13.3 mA (kW)	4.7	10.35	18.6	36.27	56.11	
Coupler Power @100 mA (kW)	35.30	77.80	139.80	272.70	421.90	
No. of Cavities / RF Generator	1	2	2	2	3	
No. of RF Generators / Section	32	24	24	20	31	131
Magnet Type	SC Solenoid	SC Solenoid	SC Solenoid	SC Solenoid	RT Quad Doublet	
Magnet Field / Gradient	1.80 - 2.32 T	2.50 - 4.00 T	4.00 - 5.40 T	4.00 - 5.63 T	4.85 - 6.05 T/m	
Average RE Gradient	0.206	0.602	1.182	1.573	2.030	1.495
Total Length Sections 1 - 4 (m)					205.246	

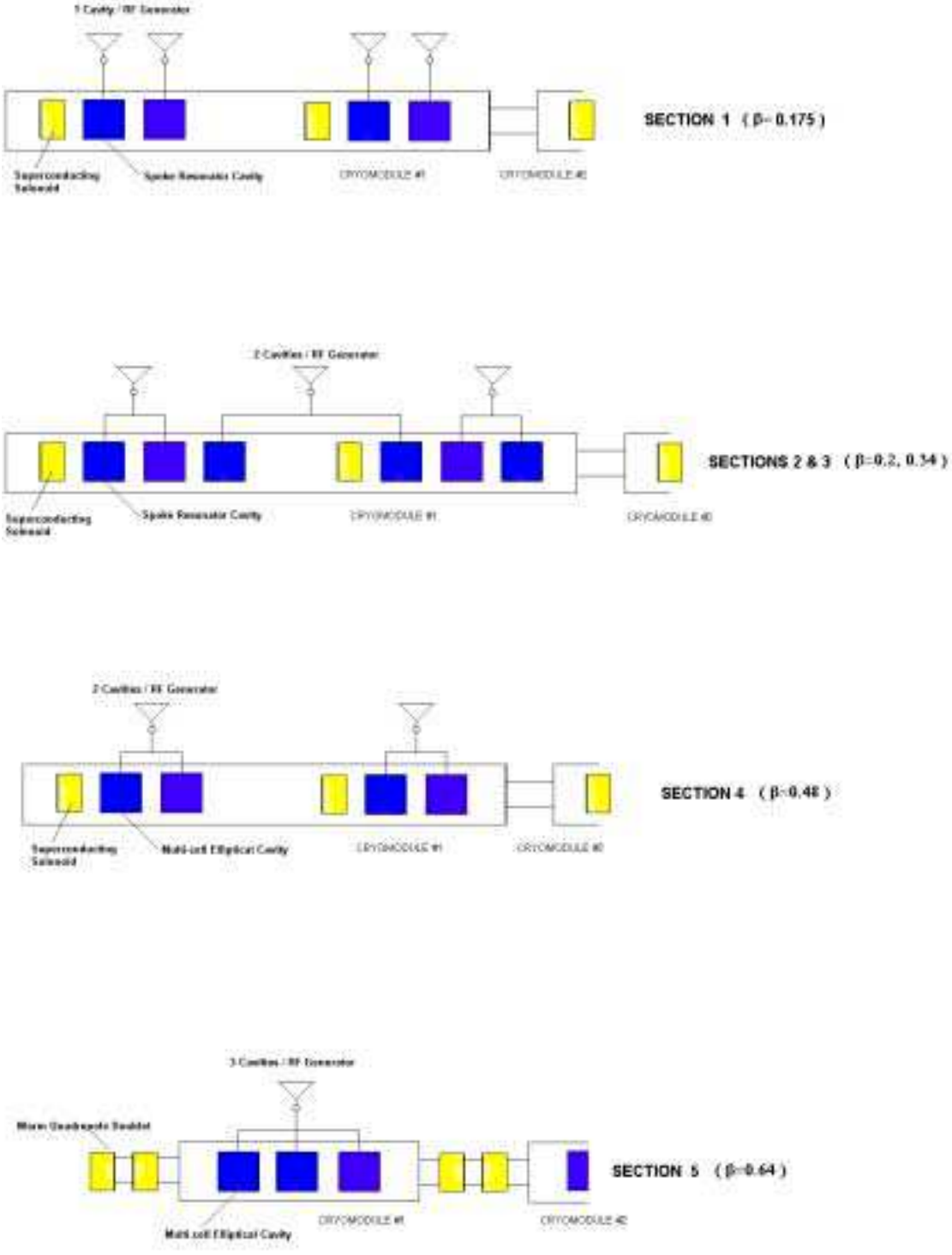

Figure 1 – Schematic cryomodule layout for each superconducting linac section.

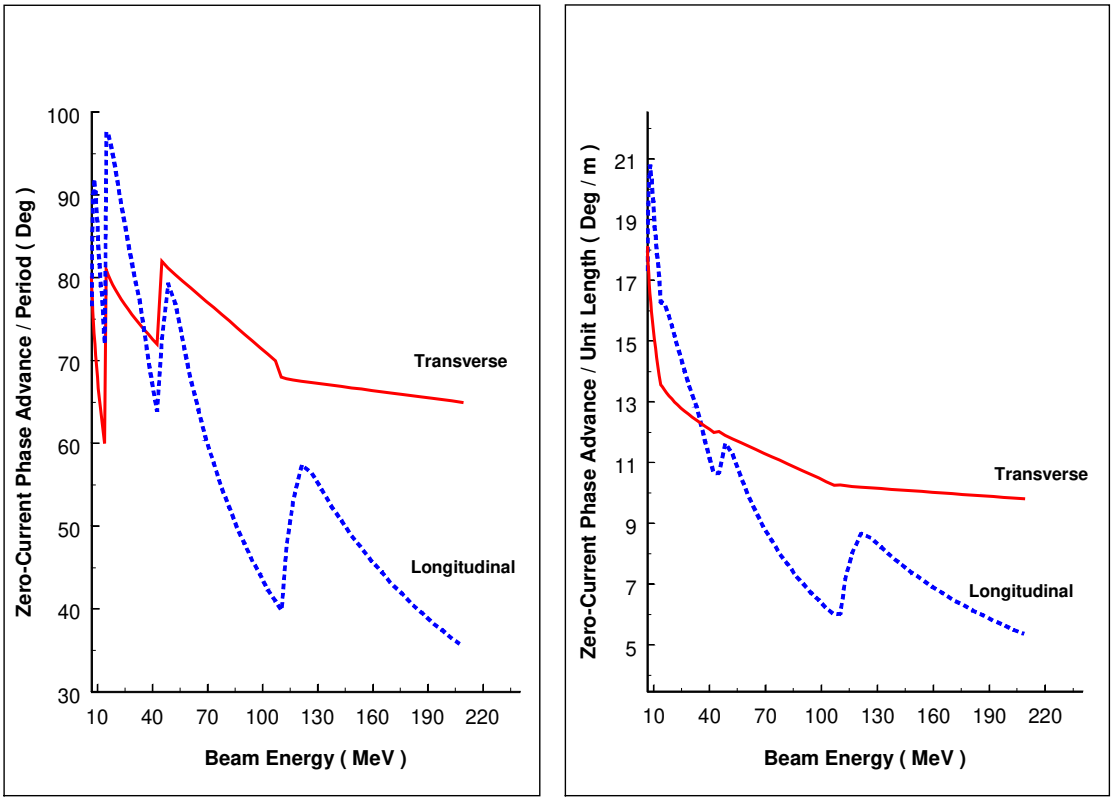

Figure 2 – Transverse and longitudinal phase advances as a function of beam energy along the linac.

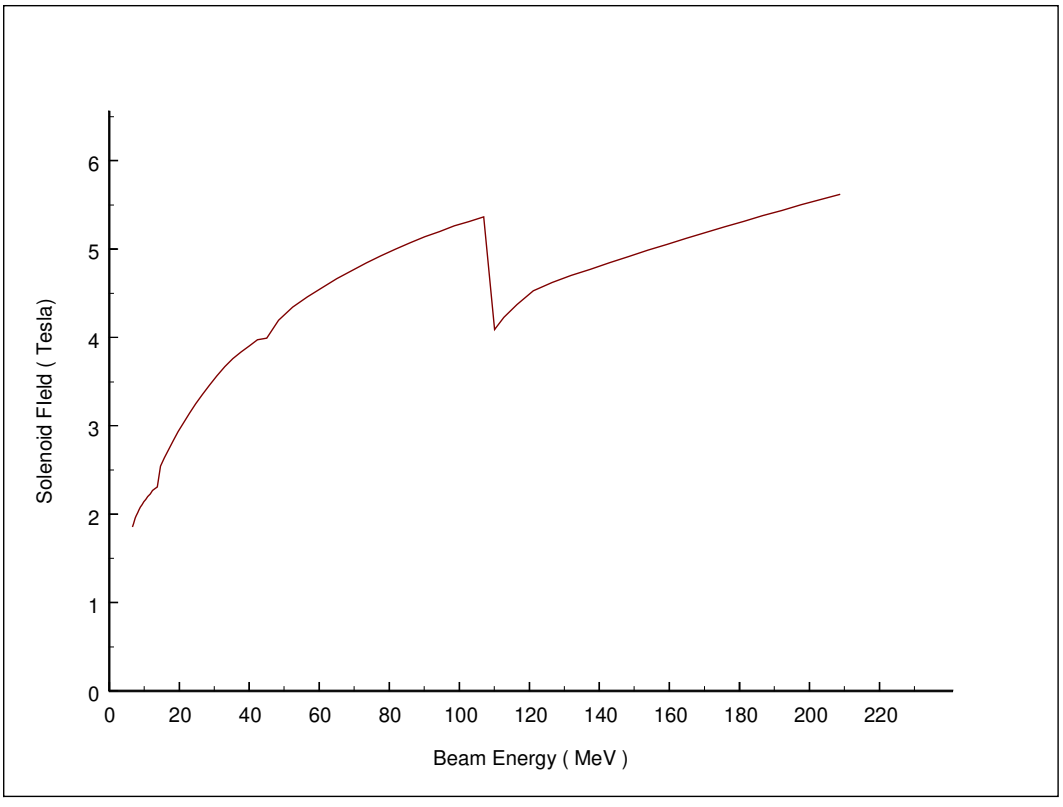

Figure 3 – Superconducting solenoid field as a function of beam energy along the linac.

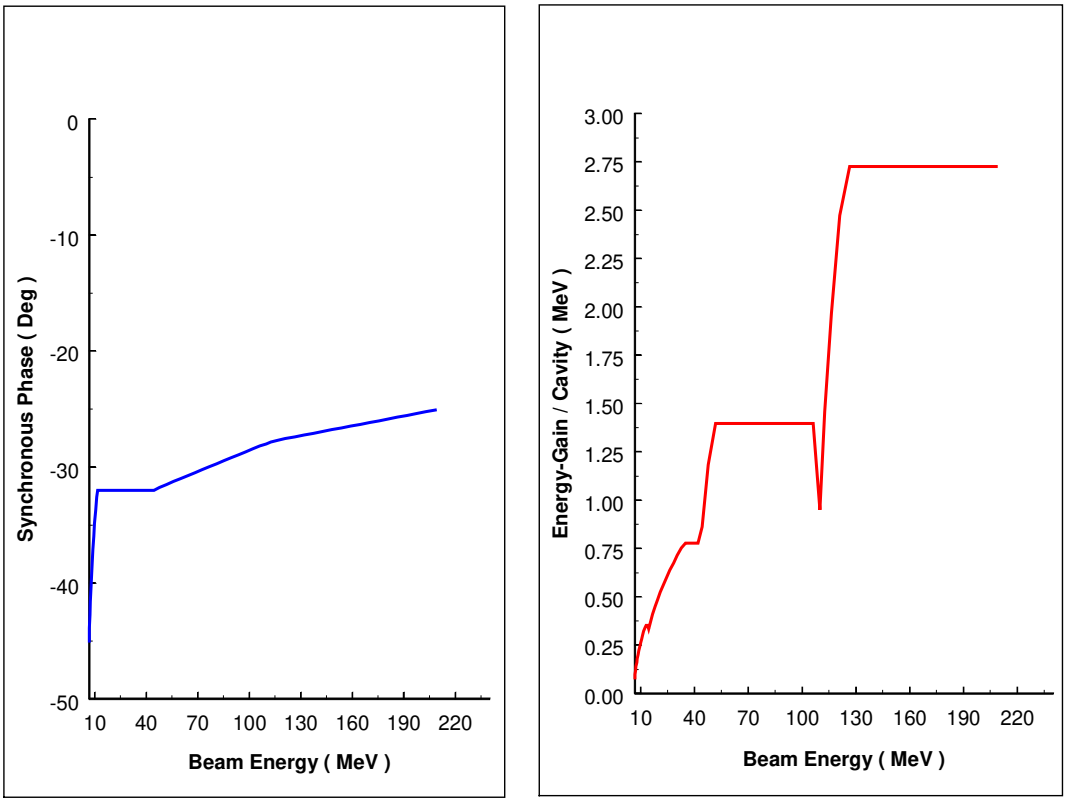

Figure 4 – Synchronous phase and energy-gain ramps as a function of energy along the linac.

In order to match the RFQ output distribution to the SC linac, each beam distribution was transformed to have the rms-matched-beam Twiss parameters as determined by running TRACE 3-D for the specific beam current. Appendix C shows the TRACE 3-D matched input beam parameters for the three beam currents. As mentioned earlier, work to design a matching section to match the RFQ output beam to the SC linac is presently in progress.

Figure 5 shows the maximum beam sizes plotted as a function of beam energy along the SC linac for 0 mA, 13.3 mA, and 100 mA. As can be seen, a large excursion of the beam is seen near 20 MeV for the 100-mA case. Examination of the simulation results showed that particles are being lost longitudially by falling out of the RF bucket, eventually becoming off-energy, and then being lost here transversely. Figure 6 shows a comparison of beam profile plots for 13.3 mA and 100 mA. The particles being lost from the RF bucket are clearly visible in the 100 mA, dW vs. distance plot. At the resolution of these simulations, 3 x 10^{-4} beam loss is observed in Section 1. The mean energy of these particles is 11.1 MeV. The total power deposited in the structures would be approximately 330 watts. We believe the relatively large longitudinal phase advance in Sec. 1 is the cause of the beam loss. We also believe that this can be corrected by using more adiabatic acceleration of the beam in Sec. 1. This can be done in the next design iteration if 100-mA operation is necessary.

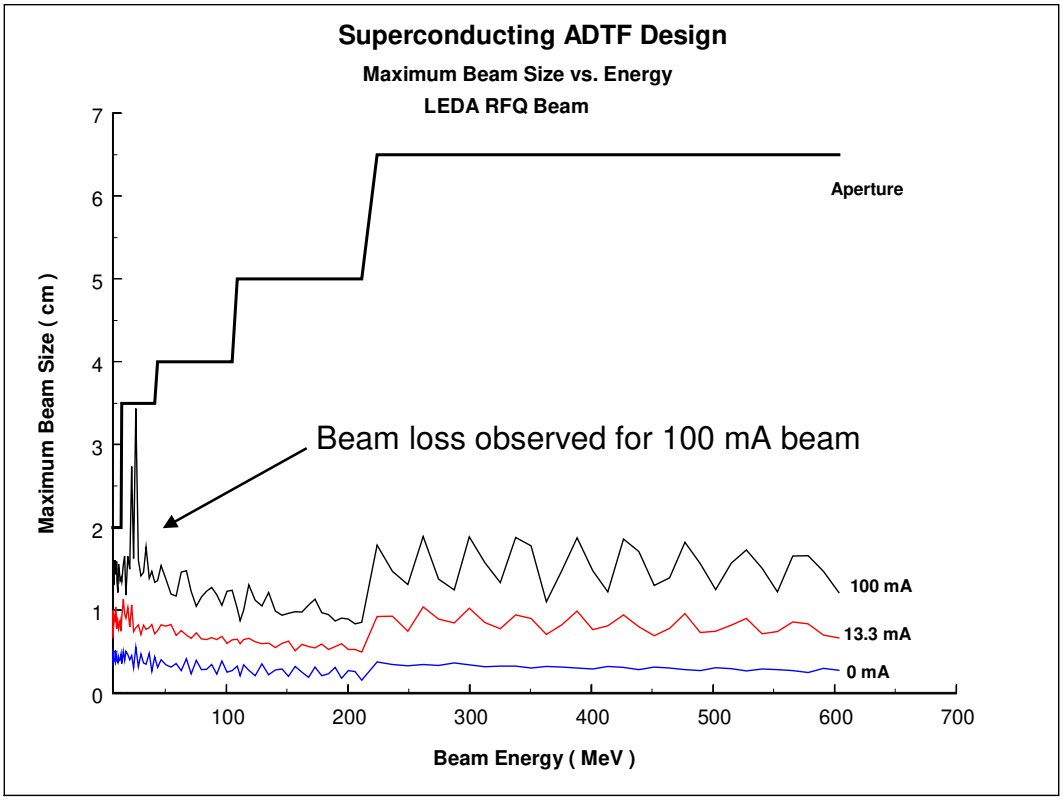

Figure 5 – Maximum beam size as a function of beam energy for 0 mA, 13.3 mA, and 100 mA.

Comparison to the Baseline APT Design

Figure 7 shows plots of the rms and maximum beam sizes at 13.3 mA for both the baseline APT design and the superconducting ADTF design for comparison. Figure 8 shows the transverse aperture-to-rms beam size ratio for the two designs. As can be seen, there is an approximately 40% improvement in the aperture-to-rms beam size ratio for the superconducting design over the APT baseline in the energy range of 50-211 MeV. This is primarily due to the larger aperture size allowed when using superconducting cavities. Figure 9 shows the transverse emittance for both cases as a function of beam energy for 13.3 mA. As can be seen, the superconducting linac demonstrates much larger emittance growth as compared to the baseline APT design. However, for both cases the maximum beam sizes and emittances are well within ranges that are easily transported to a target. The majority of the observed emittance growth is seen to occur in the low-energy part of the linac where RF defocusing and space-charge forces are the strongest. The ADTF design, by virtue of the long cryomodules, has both transverse and longitudinal focusing per unit length that is at minimum approximately 50% weaker than what is achieved in the baseline APT design between 6.7-100 MeV. This is probably the largest contributor to the observed difference in emittance growth for the two designs. Since there are no specific beam emittance requirements for ADTF and as long as the beam can be transported to the beam expander where it will be increased in size before impinging on the target, we feel this observed emittance growth is acceptable.

13.3 mA

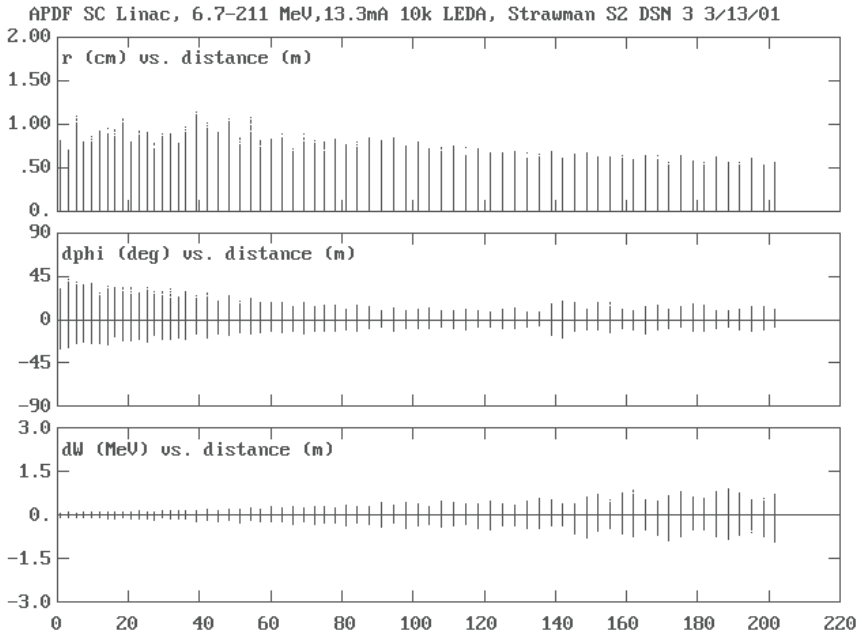

100 mA

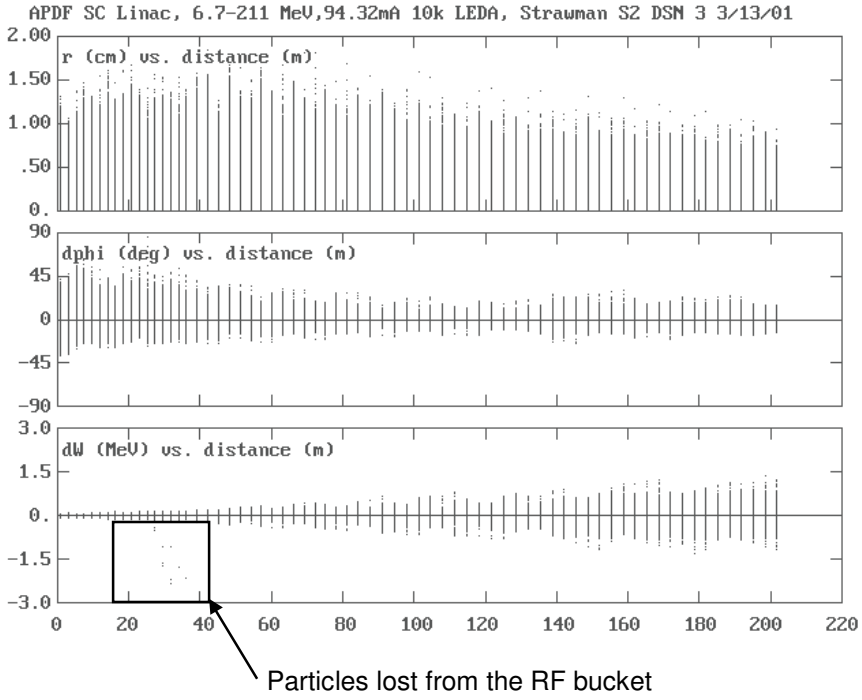

Figure 6 – Comparison of beam profile plots for 13.3 mA and 100 mA.

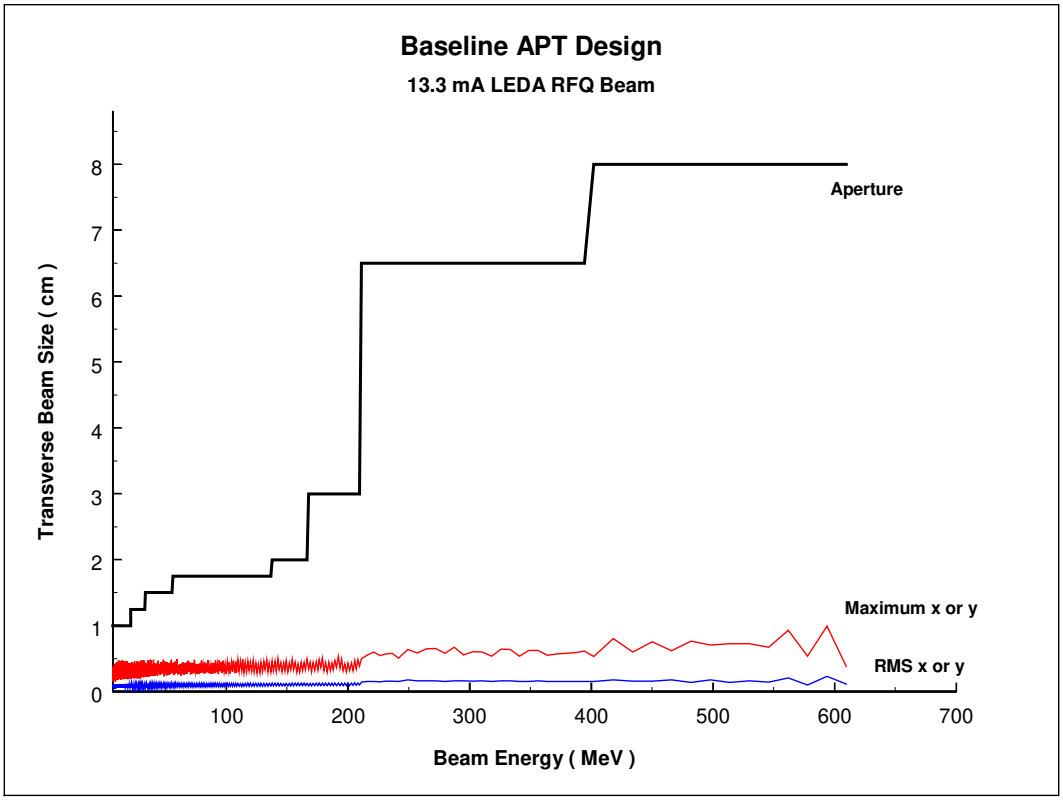

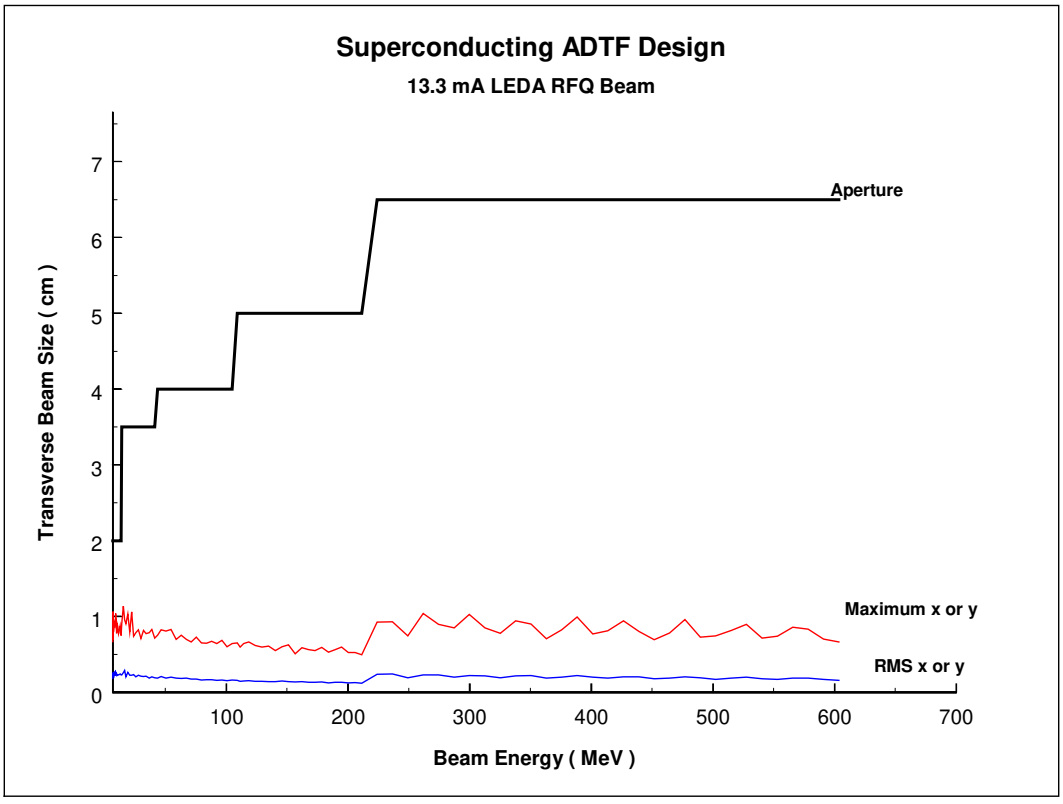

Figure 7 – Comparison of rms and maximum beam sizes at 13.3 mA for the baseline APT design and the superconducting ADTF design.

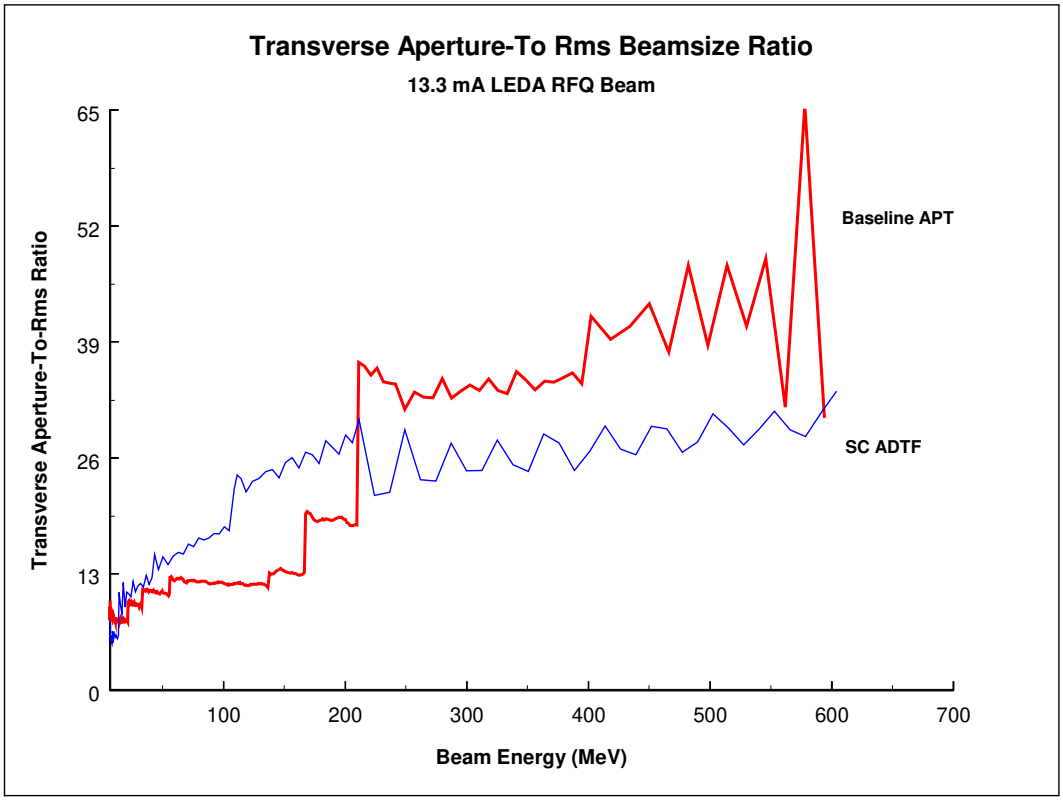

Figure 8 – Comparison of transverse aperture-to-rms beam size ratio for the two designs.

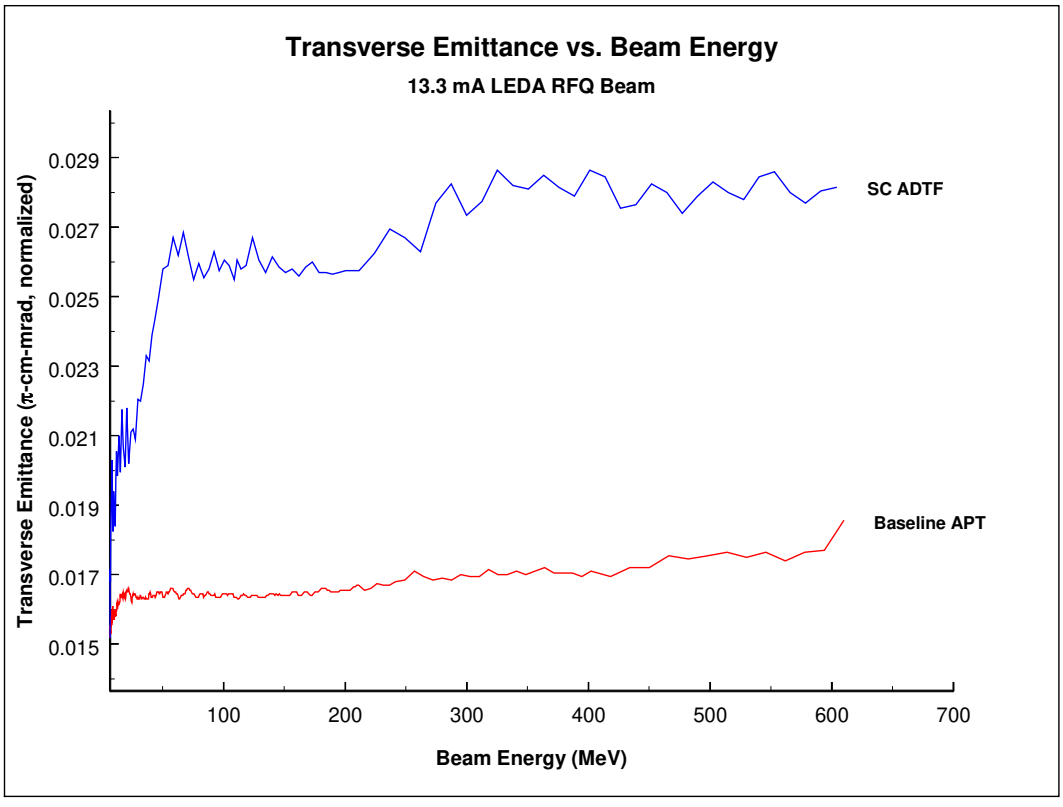

Figure 9 – Comparison of transverse emittance at 13.3 mA for the two cases.

Fault/Failure Study Results

As part of our design study we examined the effects of various faults and failures on the operation of the linac. In particular, we concentrated on two types of component faults/failures that can lead to long accelerator downtimes. Our goal was to determine the tolerances of this design to these types of failures. The first type is a magnet failure. Since we are proposing the use of superconducting solenoids throughout the majority of the linac, a failure of this type is equivalent to a magnet quench during operations. These solenoids are expected to operate in the persistence mode, where once energized, they are de-coupled from their power supply by a switch. Should a power supply fail after the solenoid has been energized, it could be repaired during operation provided the power supply is located outside of the linac tunnel. Of course, for Section 5 where it is proposed to use room-temperature quadrupole doublets between the cryomodules, a power supply failure could impact the linac operations. The second type is a RF system fault/failure. Single-cavity failures can occur due to a cavity quench, a RF window arcing, etc. Multiple-cavity failures can occur due to a RF module component failure such as a failed klystron, failure of a control system component, failed cooling water system, etc. In order to limit the scope of our study for practical reasons, the locations of failures for our study were chosen as follows:

1st solenoid of each section failed in Sections 1-4,
1st quadrupole doublet failed in Section 5,
1st RF cavity or RF module of each section failed in Sections 1-4.

These locations were also chosen because both the longitudinal and transverse lattice parameters are changing at each section-to-section transition. The idea was that a failure at the transition to a new section would introduce a larger mismatch of the beam and therefore have a more severe effect on beam quality.

Magnet Failures - Figures 10-14 show the effects of magnet failures at the various section transitions along the linac for a beam current of 13.3 mA. Our conclusion is that operation of the ideal linac appears to be tolerable to single-magnet failures. However, as can be seen, in Figs. 10 and 11, the beam size becomes relatively large in relationship to the aperture, leaving only a small margin for errors. These simulations should be repeated with the expected random alignment tolerances. It may be necessary to increase the aperture radius of the β=0.175 spoke cavities from 2.0 cm to 2.5 cm. This of course, will come at the expense of a slightly reduced transit-time factor for these cavities (probably a 10% effect). Multiple sequential magnet failures, such as the loss of both magnets in a cryomodule, were shown to result in excessively high beam losses. In this case, it is expected that the linac would be shut down for an extended period of time so that the appropriate repairs could be completed.

RF Failures - Figures 15 and 16 show the effects of a RF module failure in Section 1 and Section 2, respectively. As is shown, excessively high beam loss occurs as the result of the loss of a RF module. The effects of single-cavity failures were also examined and found to have similar results. Our conclusion is that failure of either a single accelerating cavity or a RF module (failure of multiple cavities) requires compensation so that linac operation can continue. Otherwise, linac operation must be suspended and the associated components repaired. There are essentially two options for compensating the failure of a RF module or cavity. The first option entails re-phasing all downstream cavities to compensate for the lower beam energy. This results in recapturing the beam, but the final linac output energy will be low. The second option requires re-phasing all downstream cavities, as discussed above,

with the addition of increasing the accelerating gradient of nearby cavities to restore the beam energy to its nominal value. Several combinations using upstream cavities, downstream cavities, or both upstream and downstream cavities near the failed cavities can be used. The number of cavities required to compensate depends on both the operating parameters of the failed cavities (magnitude of beam energy that will need to be restored) and the operating parameters of the nearby cavities (cavity gradients limited by peak fields). We envision the following compensation procedure to be implemented into the control system:

1. The failed cavities are detected by the control system.
2. Beam injection into the linac is terminated. Simultaneously, the failed cavities are mechanically de-tuned and the control system is using a table lookup to determine new operating phase and amplitude set points.
3. Beam injection is then resumed, therefore resuming linac operation.

Figure 17 shows beam profile plots for the nominal no failure case for comparison. Figures 18-21 show beam profile plots for the results of compensating for a single RF module failure in Sections 1-4 of the superconducting linac using downstream cavities to correct the beam energy. All downstream cavities have been re-phased. Past studies have shown that restoration of the beam to the nominal energy as near in the linac as possible to the failed cavities results in the minimum beam mismatch. As can be seen in the figures, no beam losses are observed. Additionally, only slight phase and energy oscillations are observed. These simulations should be repeated with the expected operational phase and amplitude errors. It should be noted that in these examples the minimum number of cavities was used to restore the beam to the nominal energy. For one cases this was done with a single cavity. In another case 8 cavities were required. We assumed maximum EoT values of 5 MV/m and 6 MV/m, which could not be exceeded, for Sections 1-3 and Section 4, respectively. Therefore, if several nearby cavities were operating close to these limiting values, only small incremental changes could be made to increase the energy-gain and therefore requiring more cavities.

References:

[1] R. Garnett, “AAA/ADTF April Review – Linac Beam Dynamics Talks,” Los Alamos National Laboratory Memorandum, LANSCE-1:01-041, April 12, 2001.
[2] D. Schrage, “ADTF Review,” Los Alamos National Laboratory Memorandum, LANSCE-1:01-040, April 12, 2001. See section by P. Kelley entitled, “Cryomodules and Plant.”
[3] G. Neuschaefer, “Matching Section Between the ADTF RFQ and SC Linac,” Los Alamos National Laboratory Memorandum, LANSCE-1:01-037, April 4, 2001.

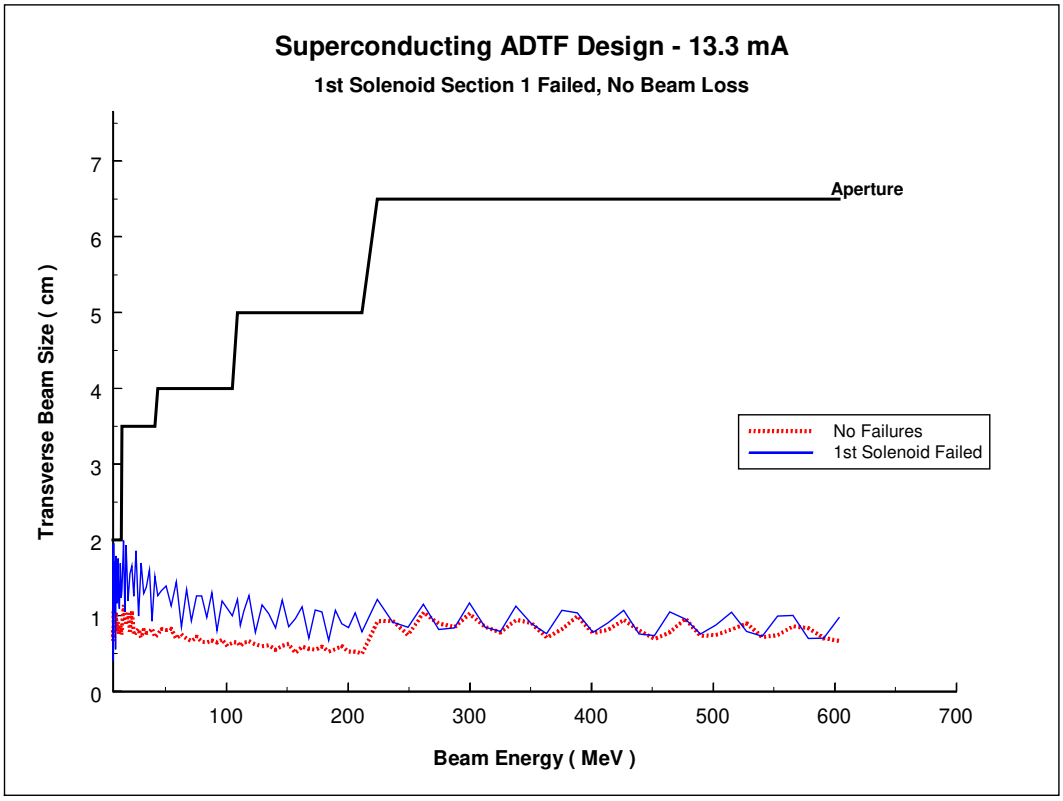

Figure 10 – Fault/Failure Study Results: First solenoid of Section 1 failed.

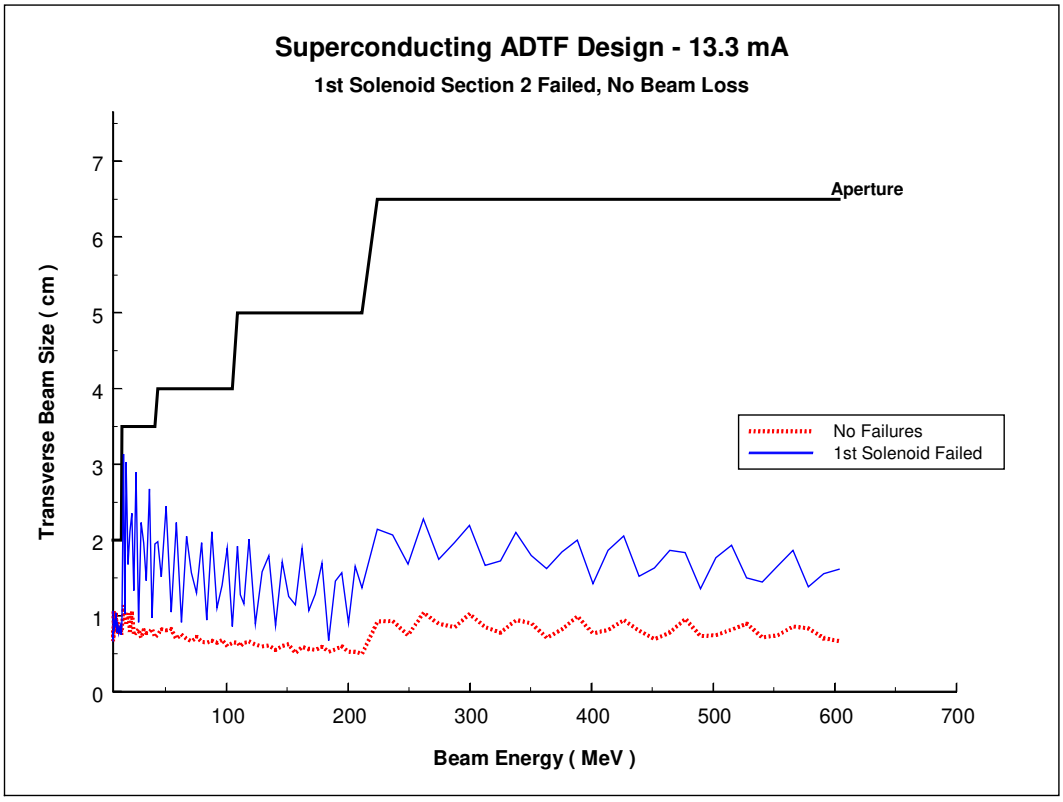

Figure 11 – Fault/Failure Study Results: First solenoid of Section 2 failed.

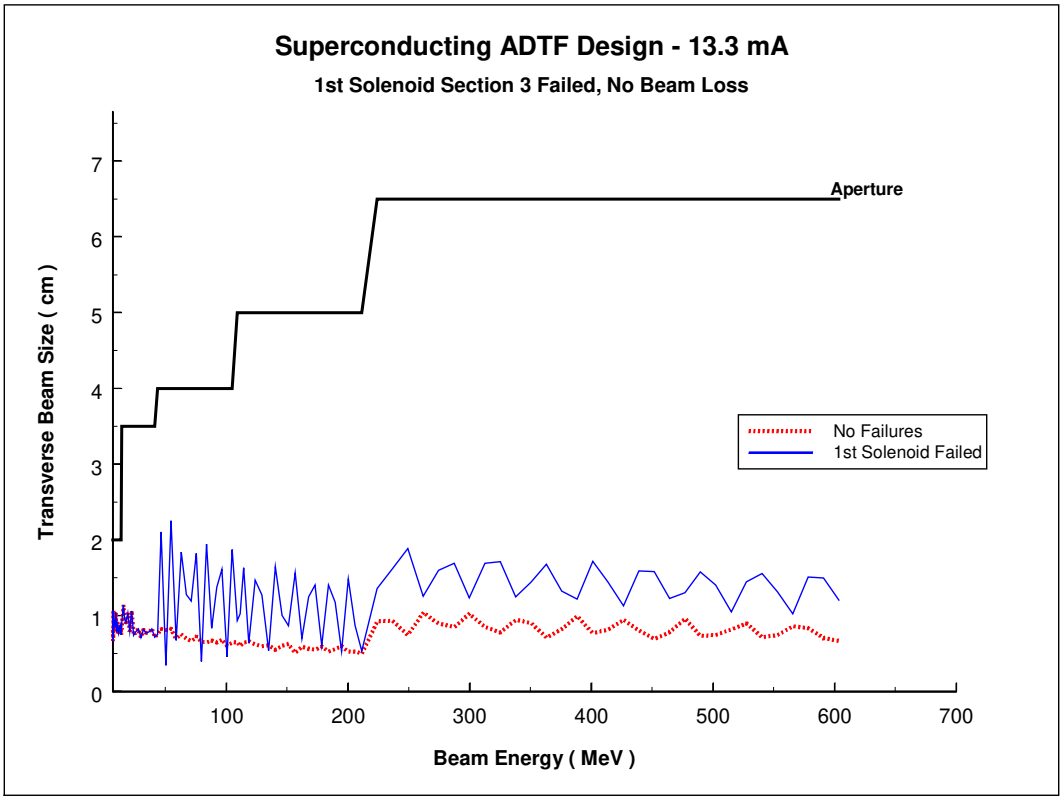

Figure 12 – Fault/Failure Study Results: First solenoid of Section 3 failed.

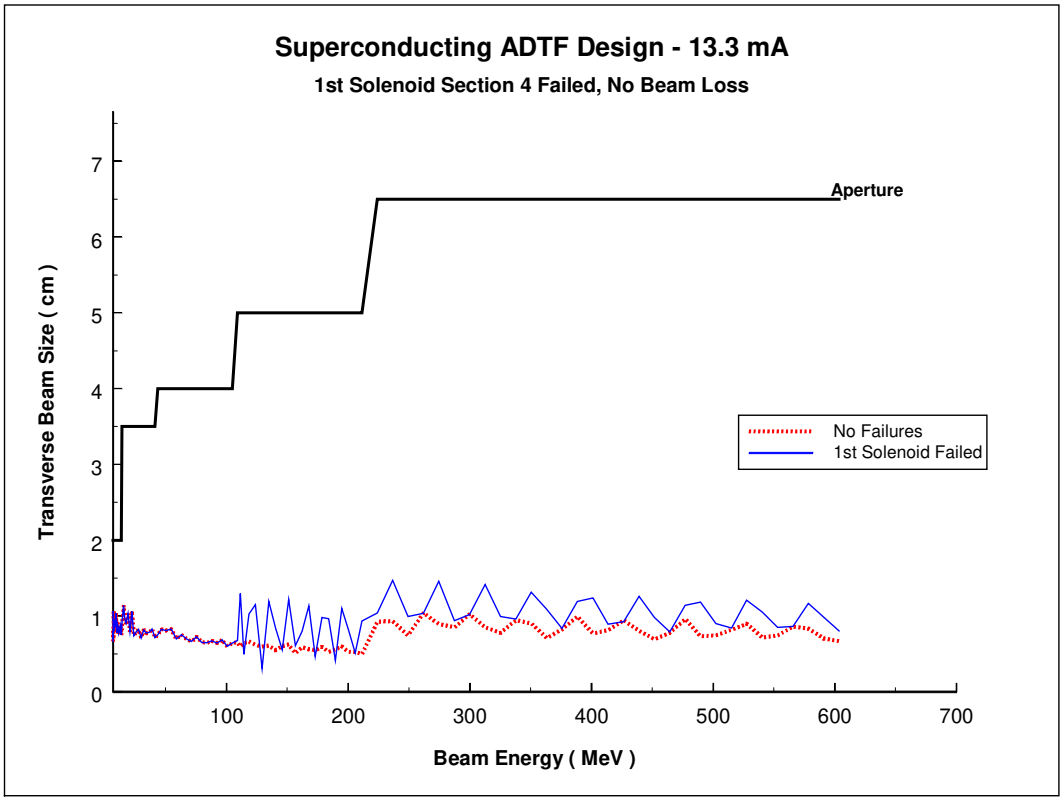

Figure 13 – Fault/Failure Study Results: First solenoid of Section 4 failed.

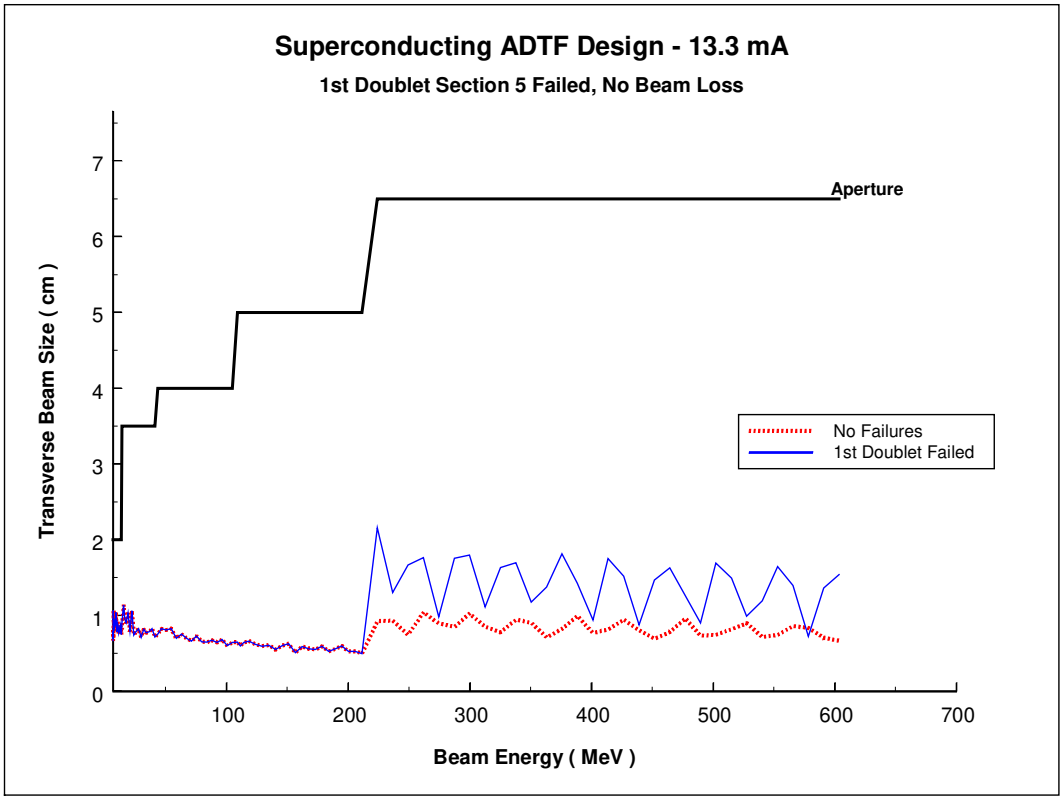

Figure 14 – Fault/Failure Study Results: First doublet of Section 5 failed.

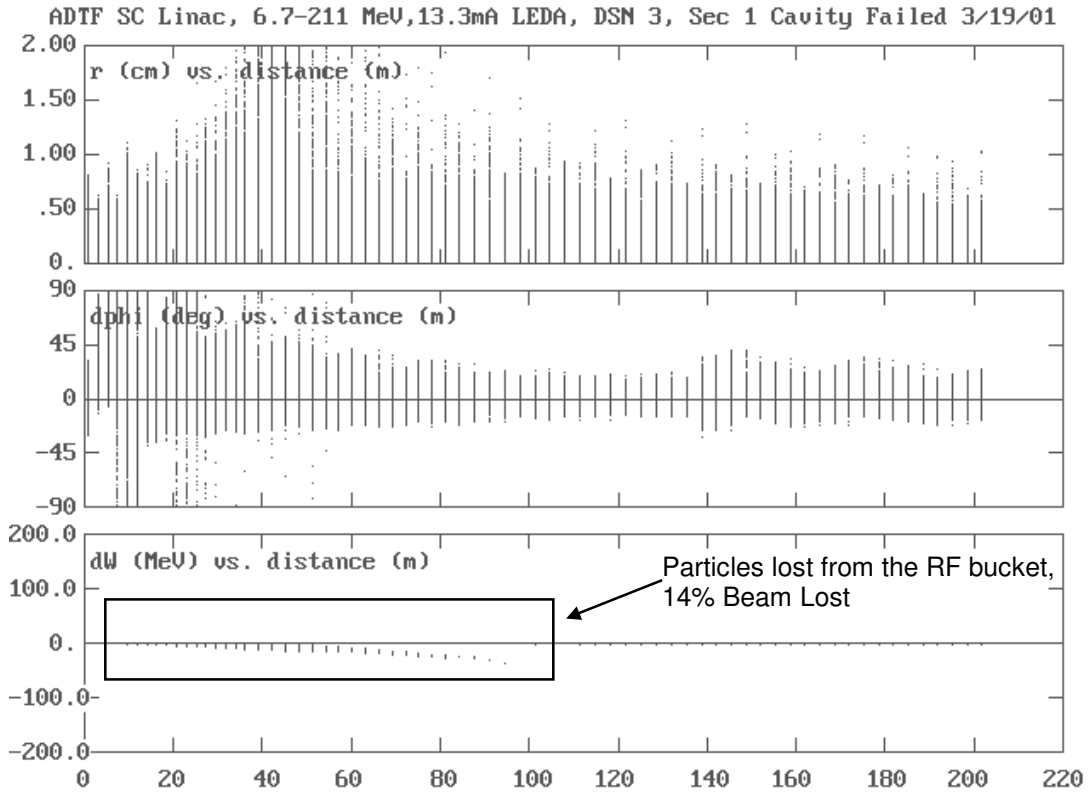

Figure 15– Fault/Failure Study Results: Uncompensated Section 1 RF module failure.

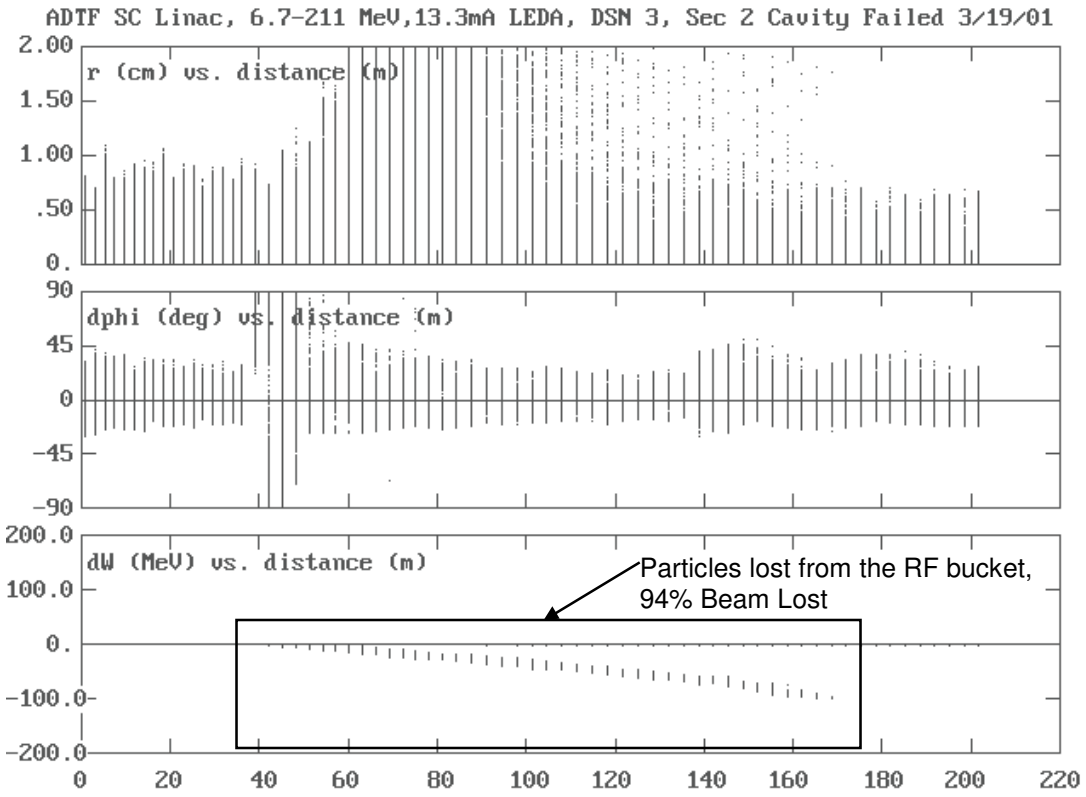

Figure 16– Fault/Failure Study Results: Uncompensated Section 2 RF module failure.

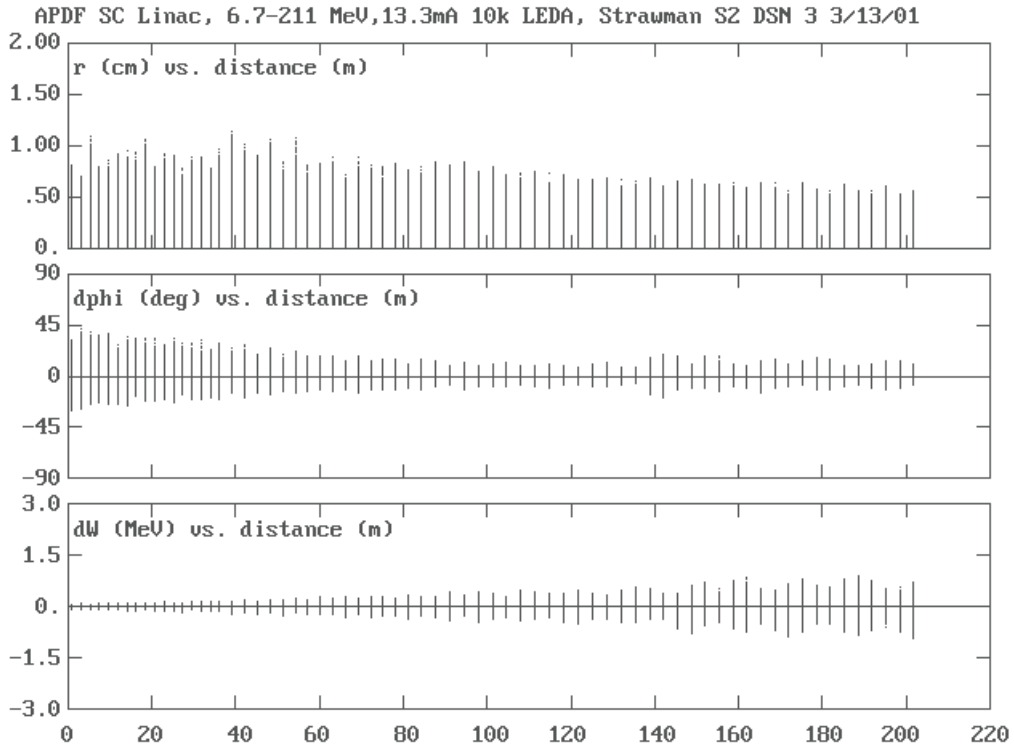

Figure 17– Beam profile plots for the nominal no RF failure case.

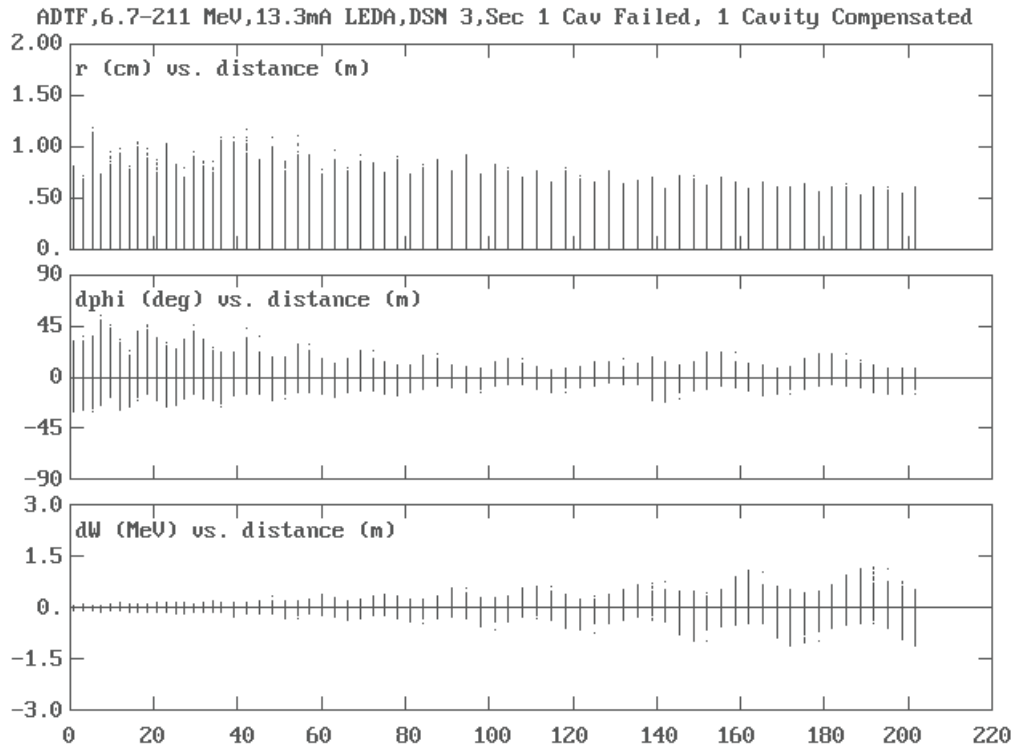

Figure 18– Compensated Section 1 RF module failure (single cavity used to compensate).

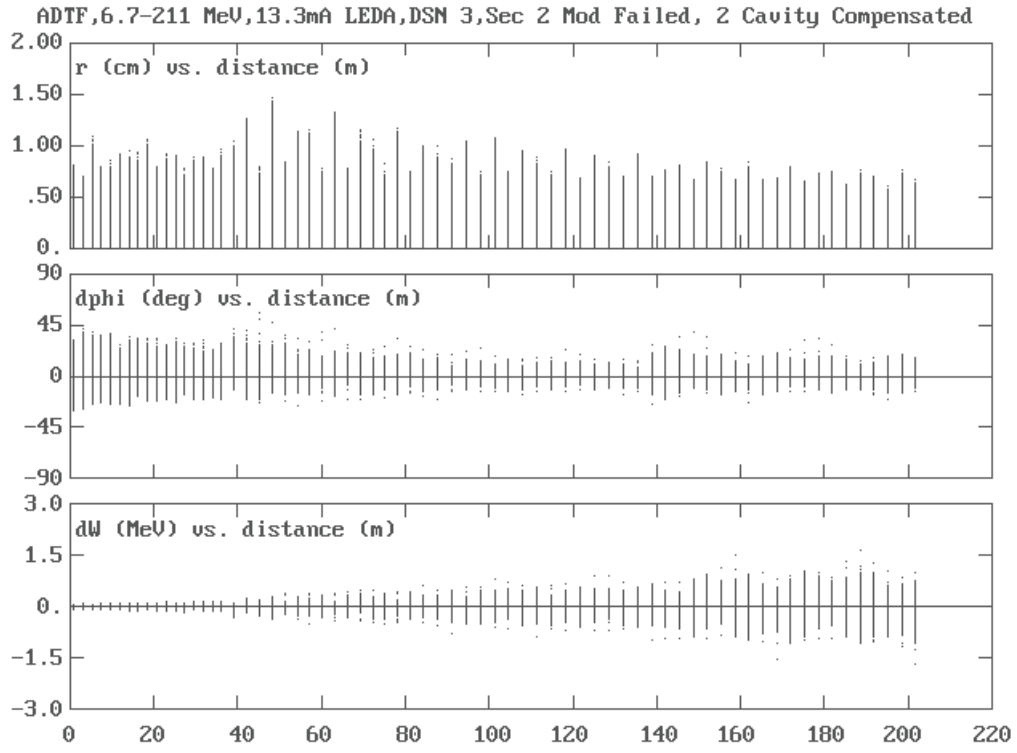

Figure 19– Compensated Section 2 RF module failure (2 cavities used to compensate).

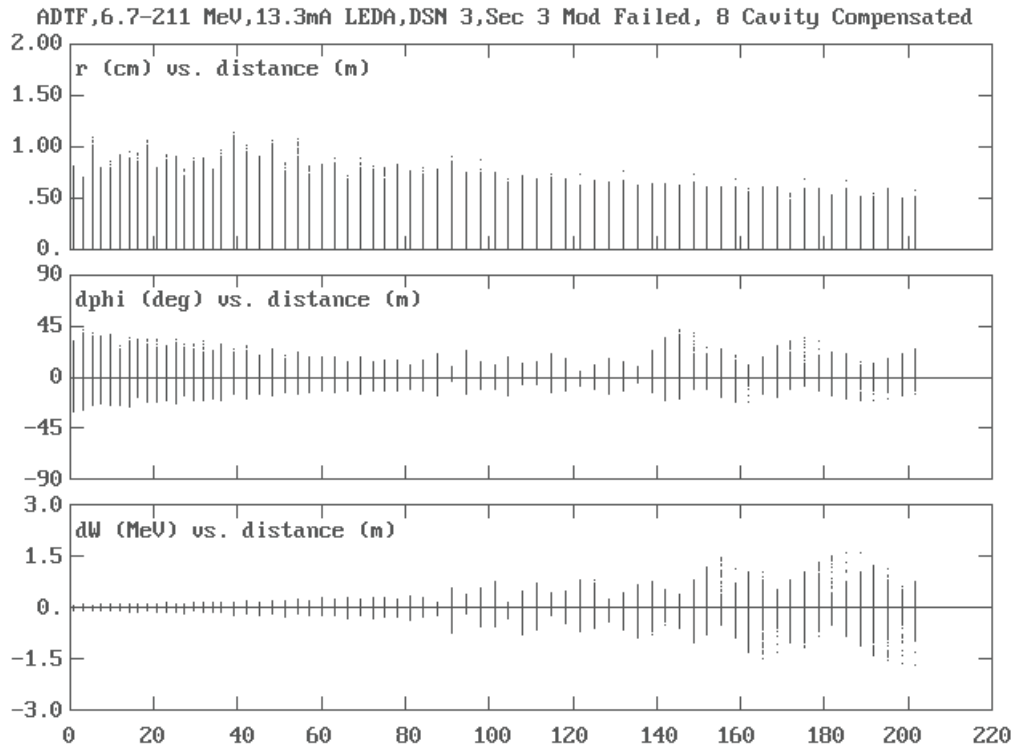

Figure 20– Compensated Section 3 RF module failure (8 cavities used to compensate).

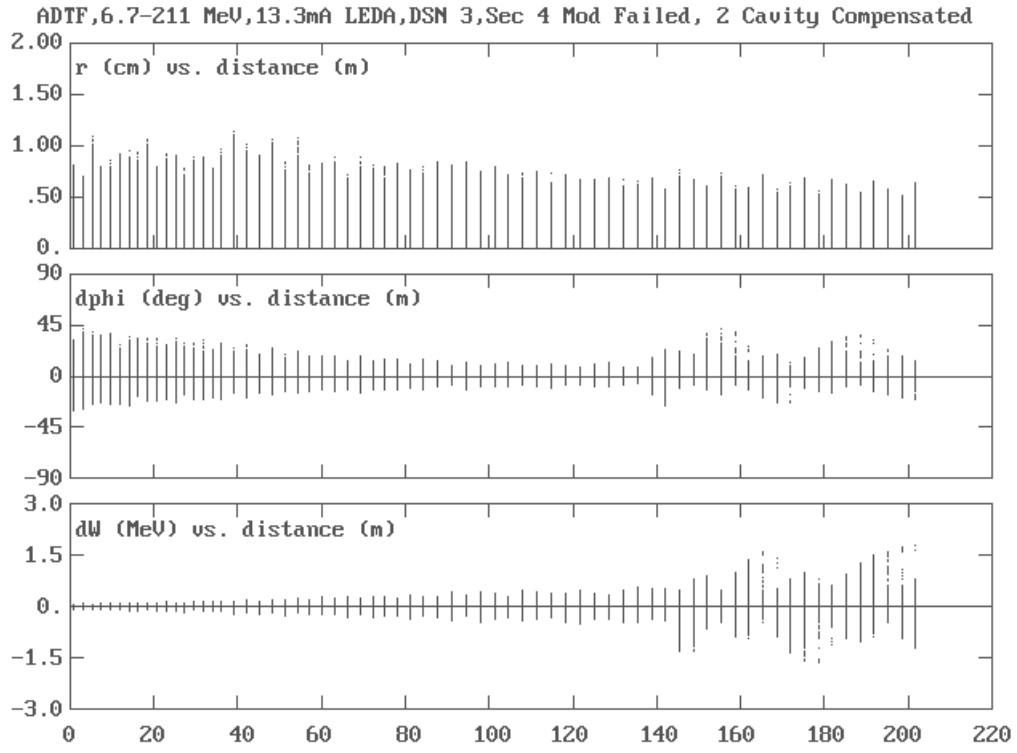

Figure 21– Compensated Section 4 RF module failure (2 cavities used to compensate).

APPENDIX A – Design Code Output File, SCLINAC.DAT

```
Superconducting Linac, number of sections =            5
 Sec     freq    BetaG  ncry  ncav  ncls  ncps  rbore   L-warm
   1   350.00    0.175     8     4     2     2  2.000    30.00
    L-w2c L-drift1 L-drift2  L-cav  L-sol  L-cryo   L-mod    L-fp
    38.10    30.00   106.20  20.00  15.00  412.40  442.40  221.20
 TTcoefs =     -3.2713    64.2821  -372.7135   949.6991  -914.0366
 cryo    Bsol   cav   kly       E0     phis      Win      Wout
    1  18638.     1     1   1.4528   -45.00     6.700     6.780
               2     2   1.5986   -44.43     6.780     6.870
    1  18962.     3     3   1.7353   -43.87     6.870     6.970
               4     4   1.8633   -43.30     6.970     7.081
    2  19229.     1     5   1.9828   -42.74     7.081     7.201
               2     6   2.0943   -42.17     7.201     7.332
    2  19575.     3     7   2.1982   -41.61     7.332     7.472
               4     8   2.2952   -41.04     7.472     7.623
    3  19842.     1     9   2.3856   -40.48     7.623     7.784
               2    10   2.4702   -39.91     7.784     7.955
    3  20205.     3    11   2.5494   -39.35     7.955     8.136
               4    12   2.6239   -38.78     8.136     8.327
    4  20465.     1    13   2.6942   -38.22     8.327     8.529
               2    14   2.7608   -37.65     8.529     8.740
    4  20836.     3    15   2.8241   -37.09     8.740     8.962
               4    16   2.8847   -36.52     8.962     9.193
    5  21079.     1    17   2.9430   -35.96     9.193     9.435
               2    18   2.9994   -35.39     9.435     9.687
    5  21449.     3    19   3.0543   -34.83     9.687     9.949
               4    20   3.1079   -34.26     9.949    10.221
    6  21662.     1    21   3.1606   -33.70    10.221    10.503
               2    22   3.2127   -33.13    10.503    10.796
    6  22022.     3    23   3.2644   -32.57    10.796    11.098
               4    24   3.3160   -32.00    11.098    11.411
    7  22299.     1    25   3.3882   -32.00    11.411    11.733
               2    26   3.4610   -32.00    11.733    12.066
    7  22696.     3    27   3.5345   -32.00    12.066    12.409
               4    28   3.6088   -32.00    12.409    12.762
    8  22939.     1    29   3.5819   -32.00    12.762    13.115
               2    30   3.5581   -32.00    13.115    13.468
    8  23101.     3    31   3.5370   -32.00    13.468    13.821
               4    32   3.5184   -32.00    13.821    14.174
 Sec     freq    BetaG  ncry  ncav  ncls  ncps  rbore   L-warm
   2   350.00    0.200     8     6     3     3  3.500    30.00
    L-w2c L-drift1 L-drift2  L-cav  L-sol  L-cryo   L-mod    L-fp
    38.10    30.00   106.20  29.60  15.00  570.00  600.00  300.00
 TTcoefs =     -6.6488    97.5510  -466.5161   968.4802  -753.4869
 cryo    Bsol   cav   kly       E0     phis      Win      Wout
    9  25458.     1    33   2.5462   -32.00    14.174    14.509
               2    33   2.5799   -32.00    14.509    14.857
               3    34   2.6140   -32.00    14.857    15.217
    9  26405.     4    34   2.6485   -32.00    15.217    15.590
               5    35   2.6838   -32.00    15.590    15.976
               6    35   2.7200   -32.00    15.976    16.374
```

10	27376.	1	36	2.7573	-32.00	16.374	16.785
		2	36	2.7959	-32.00	16.785	17.208
		3	37	2.8358	-32.00	17.208	17.645
10	28370.	4	37	2.8773	-32.00	17.645	18.094
		5	38	2.9204	-32.00	18.094	18.555
		6	38	2.9651	-32.00	18.555	19.029
11	29382.	1	39	3.0117	-32.00	19.029	19.516
		2	39	3.0602	-32.00	19.516	20.016
		3	40	3.1106	-32.00	20.016	20.528
11	30409.	4	40	3.1631	-32.00	20.528	21.053
		5	41	3.2177	-32.00	21.053	21.590
		6	41	3.2745	-32.00	21.590	22.141
12	31444.	1	42	3.3335	-32.00	22.141	22.703
		2	42	3.3948	-32.00	22.703	23.279
		3	43	3.4586	-32.00	23.279	23.867
12	32492.	4	43	3.5247	-32.00	23.867	24.468
		5	44	3.5933	-32.00	24.468	25.081
		6	44	3.6645	-32.00	25.081	25.707
13	33542.	1	45	3.7382	-32.00	25.707	26.346
		2	45	3.8146	-32.00	26.346	26.998
		3	46	3.8937	-32.00	26.998	27.662
13	34600.	4	46	3.9755	-32.00	27.662	28.338
		5	47	4.0600	-32.00	28.338	29.028
		6	47	4.1474	-32.00	29.028	29.730
14	35655.	1	48	4.2377	-32.00	29.730	30.445
		2	48	4.3308	-32.00	30.445	31.172
		3	49	4.4269	-32.00	31.172	31.912
14	36714.	4	49	4.5259	-32.00	31.912	32.665
		5	50	4.6279	-32.00	32.665	33.430
		6	50	4.7329	-32.00	33.430	34.208
15	37603.	1	51	4.7632	-32.00	34.208	34.986
		2	51	4.7950	-32.00	34.986	35.764
		3	52	4.8280	-32.00	35.764	36.542
15	38368.	4	52	4.8623	-32.00	36.542	37.320
		5	53	4.8977	-32.00	37.320	38.098
		6	53	4.9340	-32.00	38.098	38.876
16	39089.	1	54	4.9713	-32.00	38.876	39.654
		2	54	5.0093	-32.00	39.654	40.432
		3	55	5.0481	-32.00	40.432	41.210
16	39776.	4	55	5.0876	-32.00	41.210	41.988
		5	56	5.1277	-32.00	41.988	42.766
		6	56	5.1683	-32.00	42.766	43.544

Sec	freq	BetaG	ncry	ncav	ncls	ncps	rbore	L-warm
3	350.00	0.340	8	6	3	3	4.000	30.00

L-w2c	L-drift1	L-drift2	L-cav	L-sol	L-cryo	L-mod	L-fp
38.10	30.00	106.20	43.30	15.00	652.20	682.20	341.10

TTcoefs =	-8.3660	77.9774	-245.2018	338.8170	-176.7560

cryo	Bsol	cav	kly	E0	phis	Win	Wout
17	39945.	1	57	3.5224	-32.00	43.544	44.407
		2	57	3.8974	-31.91	44.407	45.377
		3	58	4.2588	-31.83	45.377	46.454
17	41979.	4	58	4.6081	-31.74	46.454	47.638
		5	59	4.9470	-31.66	47.638	48.929

		6	59	5.2775	-31.57	48.929	50.327
18	43466.	1	60	5.2059	-31.49	50.327	51.725
		2	60	5.1437	-31.40	51.725	53.123
		3	61	5.0899	-31.32	53.123	54.521
18	44617.	4	61	5.0433	-31.23	54.521	55.919
		5	62	5.0032	-31.15	55.919	57.317
		6	62	4.9686	-31.06	57.317	58.715
19	45642.	1	63	4.9391	-30.98	58.715	60.113
		2	63	4.9141	-30.89	60.113	61.511
		3	64	4.8931	-30.81	61.511	62.909
19	46655.	4	64	4.8757	-30.72	62.909	64.307
		5	65	4.8615	-30.64	64.307	65.705
		6	65	4.8503	-30.55	65.705	67.103
20	47553.	1	66	4.8417	-30.47	67.103	68.501
		2	66	4.8355	-30.38	68.501	69.899
		3	67	4.8315	-30.30	69.899	71.297
20	48446.	4	67	4.8295	-30.21	71.297	72.695
		5	68	4.8293	-30.13	72.695	74.093
		6	68	4.8308	-30.04	74.093	75.491
21	49236.	1	69	4.8338	-29.96	75.491	76.889
		2	69	4.8382	-29.87	76.889	78.287
		3	70	4.8439	-29.79	78.287	79.685
21	50029.	4	70	4.8508	-29.70	79.685	81.083
		5	71	4.8588	-29.62	81.083	82.481
		6	71	4.8677	-29.53	82.481	83.879
22	50716.	1	72	4.8776	-29.45	83.879	85.277
		2	72	4.8883	-29.36	85.277	86.675
		3	73	4.8999	-29.28	86.675	88.073
22	51416.	4	73	4.9121	-29.19	88.073	89.471
		5	74	4.9250	-29.11	89.471	90.869
		6	74	4.9385	-29.02	90.869	92.267
23	52009.	1	75	4.9525	-28.94	92.267	93.665
		2	75	4.9671	-28.85	93.665	95.063
		3	76	4.9822	-28.77	95.063	96.461
23	52629.	4	76	4.9977	-28.68	96.461	97.859
		5	77	5.0136	-28.60	97.859	99.257
		6	77	5.0300	-28.51	99.257	100.655
24	53139.	1	78	5.0466	-28.43	100.655	102.053
		2	78	5.0636	-28.34	102.053	103.451
		3	79	5.0809	-28.26	103.451	104.849
24	53675.	4	79	5.0985	-28.17	104.849	106.247
		5	80	5.1163	-28.09	106.247	107.645
		6	80	5.1343	-28.00	107.645	109.043

Sec	freq	BetaG	ncry	ncav	ncls	ncps	rbore	L-warm
4	700.00	0.480	10	4	5	2	5.000	30.00

L-w2c	L-drift1	L-drift2	L-cav	L-sol	L-cryo	L-mod	L-fp
38.10	10.00	106.20	90.00	25.00	632.40	662.40	331.20

TTcoefs = 9.6658 -105.2682 382.0002 -558.4483 286.9437

cryo	Bsol	cav	kly	E0	phis	Win	Wout
25	40928.	1	81	4.1166	-28.00	109.043	109.993
		2	81	5.1375	-27.92	109.993	111.197
25	42298.	3	82	6.1105	-27.85	111.197	112.655
		4	82	7.0323	-27.77	112.655	114.366

26	43725.	1	83	7.9023	-27.69	114.366	116.332
		2	83	8.7218	-27.62	116.332	118.551
26	45279.	3	84	9.4947	-27.54	118.551	121.024
		4	84	10.2260	-27.46	121.024	123.751
27	46230.	1	85	10.0016	-27.38	123.751	126.478
		2	85	9.8043	-27.31	126.478	129.205
27	47002.	3	86	9.6309	-27.23	129.205	131.932
		4	86	9.4787	-27.15	131.932	134.659
28	47714.	1	87	9.3453	-27.08	134.659	137.386
		2	87	9.2289	-27.00	137.386	140.113
28	48455.	3	88	9.1277	-26.92	140.113	142.840
		4	88	9.0403	-26.85	142.840	145.567
29	49139.	1	89	8.9654	-26.77	145.567	148.294
		2	89	8.9020	-26.69	148.294	151.021
29	49854.	3	90	8.8491	-26.62	151.021	153.748
		4	90	8.8058	-26.54	153.748	156.475
30	50512.	1	91	8.7715	-26.46	156.475	159.202
		2	91	8.7454	-26.38	159.202	161.929
30	51201.	3	92	8.7271	-26.31	161.929	164.656
		4	92	8.7159	-26.23	164.656	167.383
31	51837.	1	93	8.7115	-26.15	167.383	170.110
		2	93	8.7133	-26.08	170.110	172.837
31	52502.	3	94	8.7211	-26.00	172.837	175.564
		4	94	8.7345	-25.92	175.564	178.291
32	53116.	1	95	8.7532	-25.85	178.291	181.018
		2	95	8.7768	-25.77	181.018	183.745
32	53761.	3	96	8.8051	-25.69	183.745	186.472
		4	96	8.8380	-25.62	186.472	189.199
33	54355.	1	97	8.8750	-25.54	189.199	191.926
		2	97	8.9161	-25.46	191.926	194.653
33	54979.	3	98	8.9610	-25.38	194.653	197.380
		4	98	9.0095	-25.31	197.380	200.107
34	55554.	1	99	9.0614	-25.23	200.107	202.834
		2	99	9.1166	-25.15	202.834	205.561
34	56159.	3	100	9.1749	-25.08	205.561	208.288
		4	100	9.2360	-25.00	208.288	211.015

APPENDIX B – LINAC Code Input Files

LINAC.DAT:

```
  350.000     6.700  938.2796    1.0000        0    4    0
```

LINAC.INP:

```
 ADTF 350=MHz SC Linac, Strawman S2 Dsn 3 2/13/01
 &run  nm1=  1, nm2= 36, de= 100., mprnt=1,
 fmod(1)=500*1., ntpm=36*1
    rmesh=1.0,zmesh=2.,nr=20,nz=40,nip=0,frm=1.2,xi=0.,
   nruns= 1, lprn=1, ifringe=1, ienergy=1, isteer=0, noprint=1
   locout=2,
 iout=  9,optcon(1)=  220.,11,2., 2, 90.0, 0., 3.0, 1 &
 LEDA 13.3mA RFQ Distr Input at 6.7 MeV
 &inp nn=8, vv = 12, 35.80131,-0.716,263.24,-0.722,265.21,
   -0.295,499.56  &end
   APDF SC Linac, 6.7-211 MeV,13.3mA 10k LEDA, Strawman S2 DSN 3 3/13/01
 &run iend=1 &end

**********************************************************************

 iout=  9,optcon(1)=  200.,6,3., 2, 90.0, 0., 3.0, 1 &
 iout=  7,optcon(1)=  3., 2, 10.0, 2, -90., 2., 1.0, 2 &
```

APPENDIX C – TRACE 3-D Input Match

1. Matched beam parameters for 0 mA

```
11:27:06.58 03/14/01
All longitudinal beta & emittance are for a frequency of    350.000 MHz
Current=      0.00 mA, charge= 1.0 , erest=    938.2800000 MeV    n1,n2=    1,   12

Beam energy=     6.700 MeV, V/C=0.11886936 , V/C * C/freq =   10.1818 cm, gamma= 1.00714073
PARMILA unnormalized total input units:  cm/rad cm*rad
beami=      -0.461600     153.018072      -0.461599     153.019483       0.260119     151.789260
temporary long. beta and long. emit(3d)=     150.006950    0.002984664
emiti.3D-uniform=     0.000535600    0.000524400    0.002949618
emiti.6D-waterbag=    0.000856960    0.000839040    0.004719388
emiti.3sig-gauss =    0.000964080    0.000943920    0.005309312
dp.3D-uniform= +- 23.7 deg, dz=+- 0.6691190 cm, dw=+- 0.0616910 MeV
dp.6D-waterbag=+- 29.9 deg, dz=+- 0.8463761 cm, dw=+- 0.0780337 MeV
dp.3sig-gauss =+- 25.1 deg, dz=+- 0.7097079 cm, dw=+- 0.0654332 MeV

Beam energy=     6.870 MeV, V/C=0.12035175 , V/C * C/freq =   10.3087 cm, gamma= 1.00732191
PARMILA unnormalized total input units:  cm/rad cm*rad
beamo=      -0.461591     153.018080      -0.461587     153.016866       0.260119     157.619062
emito.3D-uniform=     0.000528654    0.000520514    0.002956647
emito.6D-waterbag=    0.000845846    0.000832822    0.004730635
emito.3sig-gauss =    0.000951577    0.000936925    0.005321964
dp.3D-uniform= +- 23.8 deg, dz=+- 0.6826594 cm, dw=+- 0.0621662 MeV
dp.6D-waterbag=+- 30.2 deg, dz=+- 0.8635035 cm, dw=+- 0.0786347 MeV
dp.3sig-gauss =+- 25.3 deg, dz=+- 0.7240697 cm, dw=+- 0.0659372 MeV

Beam energy=     6.700 MeV, PARMILA rms output units:  cm/mrad(u) cm*mrad(n), deg/MeV(n) deg*MeV(n)
beami=      -0.461600       0.153018      -0.461599       0.153019      -0.260119     396.258132
emiti.rms=    0.012824211    0.012556042    0.282500000
emiti.rms.normalized.longitudinal(cm mrad)=    0.071636794

Beam energy=     6.870 MeV, PARMILA rms output units:  cm/mrad(u) cm*mrad(n), deg/MeV(n) deg*MeV(n)
beamo=      -0.461591       0.153018      -0.461587       0.153017      -0.260119     396.245276
emito.rms=    0.012818056    0.012620681    0.286859350
emito.rms.normalized.longitudinal(cm mrad)=    0.072742244

Beam energy=     6.700 MeV, TRACE3D total units:
Transverse unnormalized, mm/mrad mm*mrad; Longitudinal normalized, deg/keV deg*keV
beami=      -0.461600       1.530181      -0.461599       1.530195      -0.260119       0.396258
emiti.3D-uniform=      5.3560000      5.2440000   1412.5000000

Beam energy=     6.870 MeV, TRACE3D total units:
Transverse unnormalized, mm/mrad mm*mrad; Longitudinal normalized, deg/keV deg*keV
beamo=      -0.461591       1.530181      -0.461587       1.530169      -0.260119       0.396245
emito.3D-uniform=      5.2865394      5.2051363   1434.2967482
```

2. Matched beam parameters for 13.3 mA

12:05:52.40 03/13/01
All longitudinal beta & emittance are for a frequency of 350.000 MHz
Current= 13.28 mA, charge= 1.0 , erest= 938.2800000 MeV n1,n2= 1, 12

Beam energy= 6.700 MeV, V/C=0.11886936 , V/C * C/freq = 10.1818 cm, gamma= 1.00714073
PARMILA unnormalized total input units: cm/rad cm*rad
beami= -0.715979 263.242147 -0.721875 265.211051 0.294515 191.361465
temporary long. beta and long. emit(3d)= 189.114499 0.002124658
emiti.3D-uniform= 0.000645000 0.000628000 0.002099710
emiti.6D-waterbag= 0.001032000 0.001004800 0.003359536
emiti.3sig-gauss = 0.001161000 0.001130400 0.003779478
dp.3D-uniform= +- 22.4 deg, dz=+- 0.6338798 cm, dw=+- 0.0467690 MeV
dp.6D-waterbag=+- 28.3 deg, dz=+- 0.8018016 cm, dw=+- 0.0591586 MeV
dp.3sig-gauss =+- 23.8 deg, dz=+- 0.6723311 cm, dw=+- 0.0496060 MeV

Beam energy= 6.870 MeV, V/C=0.12035175 , V/C * C/freq = 10.3087 cm, gamma= 1.00732191
PARMILA unnormalized total input units: cm/rad cm*rad
beamo= -0.715974 263.242652 -0.721869 265.213033 0.294515 198.714198
emito.3D-uniform= 0.000638661 0.000626309 0.002117761
emito.6D-waterbag= 0.001021857 0.001002094 0.003388417
emito.3sig-gauss = 0.001149589 0.001127356 0.003811969
dp.3D-uniform= +- 22.7 deg, dz=+- 0.6487134 cm, dw=+- 0.0472747 MeV
dp.6D-waterbag=+- 28.7 deg, dz=+- 0.8205648 cm, dw=+- 0.0597983 MeV
dp.3sig-gauss =+- 24.0 deg, dz=+- 0.6880645 cm, dw=+- 0.0501424 MeV

Beam energy= 6.700 MeV, PARMILA rms output units: cm/mrad(u) cm*mrad(n), deg/MeV(n) deg*MeV(n)
beami= -0.715979 0.263242 -0.721875 0.265211 -0.294515 499.564573
emiti.rms= 0.015443644 0.015036603 0.201100000
emiti.rms.normalized.longitudinal(cm mrad)= 0.050995254

Beam energy= 6.870 MeV, PARMILA rms output units: cm/mrad(u) cm*mrad(n), deg/MeV(n) deg*MeV(n)
beamo= -0.715974 0.263243 -0.721869 0.265213 -0.294515 499.556087
emito.rms= 0.015485345 0.015185857 0.205469052
emito.rms.normalized.longitudinal(cm mrad)= 0.052103165

Beam energy= 6.700 MeV, TRACE3D total units:
Transverse unnormalized, mm/mrad mm*mrad; Longitudinal normalized, deg/keV deg*keV
beami= -0.715979 2.632421 -0.721875 2.652111 -0.294515 0.499565
emiti.3D-uniform= 6.4500000 6.2800000 1005.5000000

Beam energy= 6.870 MeV, TRACE3D total units:
Transverse unnormalized, mm/mrad mm*mrad; Longitudinal normalized, deg/keV deg*keV
beamo= -0.715974 2.632427 -0.721869 2.652130 -0.294515 0.499556
emito.3D-uniform= 6.3866073 6.2630899 1027.3452593

3. Matched beam parameters for 94.32 mA

14:21:05.06 03/13/01
All longitudinal beta & emittance are for a frequency of 350.000 MHz
Current= 94.32 mA, charge= 1.0 , erest= 938.2800000 MeV n1,n2= 1, 12

Beam energy= 6.700 MeV, V/C=0.11886936 , V/C * C/freq = 10.1818 cm, gamma= 1.00714073
PARMILA unnormalized total input units: cm/rad cm*rad
beami= -1.418289 528.890400 -1.398428 523.047692 0.395384 353.829202
temporary long. beta and long. emit(3d)= 349.674539 0.001837285
emiti.3D-uniform= 0.001089300 0.001110200 0.001815712
emiti.6D-waterbag= 0.001742880 0.001776320 0.002905139
emiti.3sig-gauss = 0.001960740 0.001998360 0.003268281
dp.3D-uniform= +- 28.3 deg, dz=+- 0.8015309 cm, dw=+- 0.0329921 MeV
dp.6D-waterbag=+- 35.8 deg, dz=+- 1.0138653 cm, dw=+- 0.0417321 MeV
dp.3sig-gauss =+- 30.1 deg, dz=+- 0.8501519 cm, dw=+- 0.0349934 MeV

Beam energy= 6.870 MeV, V/C=0.12035175 , V/C * C/freq = 10.3087 cm, gamma= 1.00732191
PARMILA unnormalized total input units: cm/rad cm*rad
beamo= -1.418320 528.891101 -1.398447 523.043854 0.395382 367.430895
emito.3D-uniform= 0.001125516 0.001140374 0.002037642
emito.6D-waterbag= 0.001800825 0.001824599 0.003260228
emito.3sig-gauss = 0.002025928 0.002052673 0.003667756
dp.3D-uniform= +- 30.2 deg, dz=+- 0.8652703 cm, dw=+- 0.0351770 MeV
dp.6D-waterbag=+- 38.2 deg, dz=+- 1.0944900 cm, dw=+- 0.0444958 MeV
dp.3sig-gauss =+- 32.0 deg, dz=+- 0.9177578 cm, dw=+- 0.0373108 MeV

Beam energy= 6.700 MeV, PARMILA rms output units: cm/mrad(u) cm*mrad(n), deg/MeV(n) deg*MeV(n)
beami= -1.418289 0.528890 -1.398428 0.523048 -0.395384 923.699733
emiti.rms= 0.026081801 0.026582223 0.173900000
emiti.rms.normalized.longitudinal(cm mrad)= 0.044097835

Beam energy= 6.870 MeV, PARMILA rms output units: cm/mrad(u) cm*mrad(n), deg/MeV(n) deg*MeV(n)
beamo= -1.418320 0.528891 -1.398447 0.523044 -0.395382 923.700182
emito.rms= 0.027289917 0.027650185 0.197695822
emito.rms.normalized.longitudinal(cm mrad)= 0.050132017

Beam energy= 6.700 MeV, TRACE3D total units:
Transverse unnormalized, mm/mrad mm*mrad; Longitudinal normalized, deg/keV deg*keV
beami= -1.418289 5.288904 -1.398428 5.230477 -0.395384 0.923700
emiti.3D-uniform= 10.8930000 11.1020000 869.5000000

Beam energy= 6.870 MeV, TRACE3D total units:
Transverse unnormalized, mm/mrad mm*mrad; Longitudinal normalized, deg/keV deg*keV
beamo= -1.418320 5.288911 -1.398447 5.230439 -0.395382 0.923700
emito.3D-uniform= 11.2551564 11.4037415 988.4791095

Distribution:

E. Arthur, AAA-PDO, H816
D. Barlow, LANSCE-1, H817
M. Cappiello, AAA-TPO, H816
D. Chan, AAA-TPO, H816
P. Colestock, LANSCE-9, H851
A. Jason, LANSCE-1, H817
D. Gilpatrick, LANSCE-1, H817
P. Kelley, LANSCE-1, H817
F. Krawczyk, LANSCE-1, H817
R. LaFave, LANSCE-1, H817
G. Lawrence, AAA-TPO, H816
M. Lynch, LANSCE-5, H827
J. McGill, AAA-TPO, H816
D. Rees, LANSCE-5, H827
L. Rybarcyk, LANSCE-1, H817
R. Sheffield, AAA-TPO, H816
E. Schmierer, ESA-DE, H821
D. Schneider, AAA-TPO, H816
D. Schrage, LANSCE-1, H817
S. Schriber, LANSCE-1, H817
V. Smith, AAA-TPO, H816
T. Tajima, LANSCE-1, H817
J. Tooker, AAA-TPO, H816
R. Valdiviez, LANSCE-1, H817
T. Wangler, LANSCE-1, H817
R. Wood, LANSCE-1, H817
AAA Project File
LANSCE-1 File